Received: 10 January 2022 | Revised: 27 April 2022 | Accepted: 17 May 2022

DOI: 10.1002/mp.15727

RESEARCH ARTICLE

MEDICAL PHYSICS

Radiation shielding assessment of high-energy proton imaging at a proton therapy facility

Scott N. Penfold[1,2]

[1]Australian Bragg Centre for Proton Therapy and Research, South Australian Health and Medical Research Institute, Adelaide, South Australia, Australia

[2]Department of Physics, University of Adelaide, Adelaide, South Australia, Australia

Correspondence
Scott N. Penfold, Australian Bragg Centre for Proton Therapy and Research, South Australian Health and Medical Research Institute, Adelaide, SA 5000, Australia.
Email: scott.penfold@sahmri.com

Abstract

Background: Proton imaging makes use of high-energy, low-intensity proton beams that fully traverse the patient and has been suggested to reduce range uncertainty in proton therapy. Upright patient positioning with proton imaging is being considered for a fixed beam room of a new proton therapy facility currently under construction. Considering that the yield and energy spectrum of secondary radiation from high-energy proton beams is proton beam energy dependent, an assessment of radiation shielding at the energies required for proton imaging should be performed prior to use. Furthermore, NCRP 144 recommends that pion production be considered for proton energies greater than 300 MeV, which are not typically utilized for proton therapy but may be required for proton imaging.

Purpose: The purpose of this work was to determine whether proton treatment and imaging with an upright patient positioning system on a fixed beamline were acceptable from a radiation shielding perspective. This is the first report on radiation shielding assessment of proton imaging applications and includes consideration of pion production at the proton beam energy of 330 MeV.

Methods: The Geant4 Monte Carlo toolkit was used for the radiation shielding assessment. The calculations consisted of the generation of secondary particle phase-space files by simulating the passage of high-energy proton beams in two target materials, and subsequent simulation of the secondary particles in the proton therapy facility geometry. Particle fluence was converted to operational and protection radiation safety quantities with a custom python script for assessment of instantaneous and annual doses, respectively.

Results: The total yields of pions from a 330-MeV proton beam were many orders of magnitude less than that of neutrons and photons. Three-dimensional maps of ambient dose rate for a 330-MeV proton beam showed doses arising from secondary neutrons and photons far exceed those arising from pion production. Incorporating representative annual workloads into the calculation demonstrated that proton imaging doses outside the shielded area were negligible compared to those arising from proton therapy.

Conclusions: Pion production has a negligible impact on the radiation shielding of proton imaging at 330 MeV relative to neutron and photon production. Radiation shielding designed for proton therapy is adequate for high-energy proton imaging applications.

KEYWORDS
proton imaging, proton therapy, proton therapy shielding, radiation safety

1 | INTRODUCTION

Proton imaging has been suggested as a means to reduce range uncertainty in proton therapy.[1] By directly measuring the stopping power of the patient at the time of treatment, proton imaging can avoid the uncertainty arising from the heuristic conversion of X-ray computed tomography Hounsfield units to proton stopping powers.[2] Proton imaging makes use of high-energy, low-intensity proton beams that fully traverse the patient. Considering that the yield and energy spectrum of secondary radiation from high-energy proton beams is proton beam energy dependent, an assessment of radiation shielding at the energies required for proton imaging should be performed prior to use.

The Australian Bragg Centre for Proton Therapy and Research (ABCPTR) is currently under construction and will house two half-gantry treatment rooms and a fixed beam room with two beamlines: one for conventional supine/prone treatments, and the other for translational research purposes. The ProTom Radiance 330 synchrotron-based system will supply high-energy protons, up to 330 MeV, to the treatment rooms. Beam delivery will be via a pencil beam scanning nozzle.

The translational research beamline at the ABCPTR was originally designed for low-energy applications, and hence the opposition of the beamline to the maze entry was acceptable. The specific purpose of this work was to determine whether proton treatment and imaging with an upright patient positioning system on this beamline was acceptable from a radiation shielding perspective. More generally, this is the first report on radiation shielding assessment of proton imaging applications for proton beam energies up to 330 MeV. The unique aspects of proton imaging in the radiation shielding assessment include workload estimates, and the inclusion of pion and muon secondary particles, which NCRP 144 recommends, be considered for proton beams greater than 300 MeV.[3]

2 | MATERIALS AND METHODS

2.1 | Facility layout

A schematic of the accelerator and fixed beam room layout is shown in Figure 1. The fixed beam room with maze contains two beamlines. The translational research beamline opposes the maze entry from the corridor. The clinical beamline will be utilized for conventional supine treatment techniques. The focus of the current work is the translational research beamline.

2.2 | Proton imaging beam parameters

2.2.1 | Beam current

Proton radiography (pRad) and tomography (pCT) make use of high-energy, low-intensity proton beams to traverse the imaged object. The intensity of the proton beam should be tuned so that the count rate capability of the detector system is not exceeded but be maintained as close as possible to the count rate limit to minimize image acquisition time. Proton imaging systems with a single-proton count rate of between 1 and 10 MHz are in development.[2] To ensure conservatism in the ambient equivalent dose rate estimate, a proton imaging beam intensity of 1×10^7 protons per second exiting the beam nozzle has been assumed in the current work.

2.2.2 | Proton imaging workload

To ensure conservatism in annual dose estimates, it is assumed all proton imaging will be acquired in pCT mode, as opposed to pRad mode. The number of protons per tomography has been estimated to be 7.5×10^8 based on the 1.5×10^7 protons used to acquire a proton tomography of a pig's head,[4] and noting that the noise levels will likely need to be reduced in the clinical setting. The conservative workload calculations also assume that every treatment fraction includes a pCT image acquisition. To incorporate an aspect of proton imaging in the QA workload, it has been assumed that an additional 10% of the clinical workload will be required during nonclinical work.

2.2.3 | Energy use factors

Although treatment beam energies are limited to 250 MeV, the ProTom Radiance 330 is capable of producing proton beam energies up to 330 MeV for proton imaging applications. Three representative beam energies were used for the Monte Carlo radiation shielding calculations: 190, 250, and 330 MeV. These proton beam energies correspond to a range in water of 23.8, 37.9, and 60.2 cm[5] under the continuous slowing down approximation and were allocated use factors of 0.4, 0.4, and 0.2, respectively.

2.3 | Monte Carlo calculations

Monte Carlo calculations were carried out with the Geant4 toolkit,[6] release 10.3. The Monte Carlo calculations were divided into two steps: creation of phase-space files for secondary neutrons, photons, and pions for each proton beam energy-target material

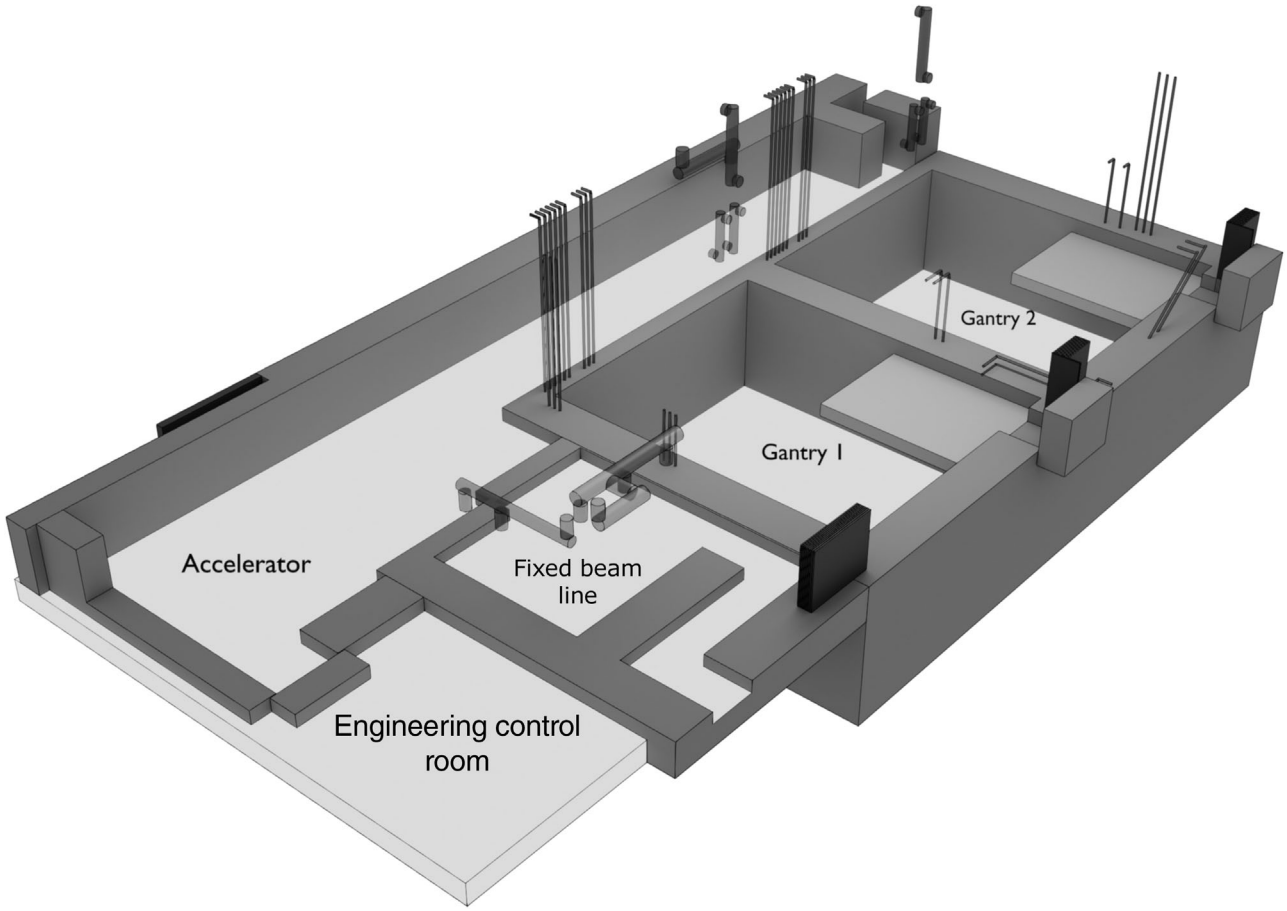

FIGURE 1 Layout of the Australian Bragg Centre for Proton Therapy and Research implemented in the radiation shielding calculations. The subsets of the major shielding concrete penetrations are shown, as well as additional shielding steel (dark).

combination, and subsequent simulation of the phase-space particles as "primary" particles in the proton therapy facility geometry. The Geant4 simulation code was validated against equivalent calculations with MCNP by an independent group during the regulatory assessment of facility shielding for proton therapy.

2.3.1 | Phase-space creation

Phase-space simulations were performed with the QGSP_BIC_HP precompiled physics list. The binary ion cascade (BIC) model has been recommended as the preferred inelastic nuclear interaction model for proton therapy applications[7] and has been validated for neutron and pion yields by Ivanchenko[8] and Bungau,[9] respectively. Neutron and photon phase-space files were generated for each proton beam energy-target material combination. Pion phase-space files were also created for the 330-MeV proton beam energy. Target materials were limited to water and copper. Water was used to represent proton interactions in the patient and residual range detector, whereas copper was used to represent beam losses in the accelerator and beam transport system at the suggestion of the proton therapy equipment vendor. The phase-space simulation was a simplified approximation of a real beam delivery with a simple pencil beam incident on a cylinder of the target material. The water target had a diameter of 10 cm, whereas the copper target had a diameter of 7 cm. The length of the target cylinder was dependent on the beam energy and chosen to minimize attenuation of secondary particles in the target.

A spherical scoring shell of 1-m radius was centered on the target and recorded the position, direction and energy of all neutrons, and photons passing through. For the 330-MeV simulations, all pion particles passing though the sensitive shell were also recorded to a phase-space file.

2.3.2 | Secondary radiation fluence simulation

A three-dimensional model of the proton therapy facility was created in Geant4 (Figure 1). The model consisted

of concrete structures forming the floor, walls, and ceiling of the shielded areas, as well as major penetrations for ventilation, and electrical conduits. Supplementary steel shielding was required in several locations to provide additional shielding.

Secondary radiation fluence simulations were performed with the QGSP_BERT_HP precompiled physics list. The Bertini cascade model was found to better reproduce neutron attenuation lengths in concrete than the BIC model that was utilized in the phase-space simulations. The Bertini cascade nuclear model is also recommended for radiation shielding applications in Geant4 by Koi.[10]

Sensitive spherical scoring volumes were distributed in a grid of 1-m spacing. The sensitive spheres were 30 cm in diameter, mimicking the size of an ICRU sphere. The spheres were created in a parallel world geometry such that the particles did not interact with the spheres, but the properties of the radiation could be queried when entering a sphere. Particle type and particle energy were recorded when entering a sphere. Ambient dose rates arising from neutron, photon, pion, and muon fluences were considered independently, as well as in combination. Although muons are not generated directly by proton nuclear interactions, they are the decay product of charged pions and may be generated with large kinetic energy.

A single simulation consisted of 1×10^6 primary particles randomly sampled from the relevant phase-space file. Multiple simulation runs were performed to reduce statistical variation in the results. At the conclusion of a simulation run, particle data recorded by the sensitive volumes was printed to file for processing.

2.4 | Fluence-to-dose conversion

ICRU 95[11] was recently introduced to reduce the variability between operational (ICRU) and protection (ICRP) radiation quantities and was utilized in this work to convert particle fluence to operational or protection quantities for each sensitive volume location. The operational quantity ambient dose was utilized for instantaneous dose rate assessment, whereas the protection quantity effective dose was utilized for annual dose assessment. Area monitoring radiation detectors are typically calibrated in terms of operational quantities, whereas personal radiation dosimeters are calibrated in terms of protection quantities.

The operational quantity ambient dose rate at each sensitive volume location was calculated with the following equation:

$$H^* = C_j \sum_{i=1}^{N_k} \frac{c_{k,H}\left(E_{k,i}\right)}{A} I \tag{1}$$

where H^* is ambient dose rate, C_j is a scaling coefficient to convert the number of Monte Carlo–simulated particles of type j to the number expected in 1 h when the system is operated at a given proton beam current I and incident on the designated target material, N_k is the number of particles of type k incident on the sensitive volume, $c_{k,H}$ is the ICRU 95 energy dependent fluence to ambient dose conversion coefficient for particle of type k, $E_{k,i}$ is the energy of the particle i, type k recorded at the sensitive volume, and A is the surface area of the 30-cm diameter spheres detecting the particle fluence.

The protection quantity effective dose at each sensitive volume location for each proton beam energy considered was calculated with the following equation:

$$E = \sum_{E_p} \left(D_j \sum_{i=1}^{N_k} \frac{c_{k,h}\left(E_{k,i}\right)}{A} W f_{E_p} \right) \tag{2}$$

where E is the annual effective dose, D_j is a scaling coefficient to convert the number of Monte Carlo–simulated particles of type j to the number expected in one year when the system is operated at an annual proton imaging workload W, N_k is the number of particles of type k incident on the sensitive volume, $c_{k,h}$ is the ICRP 116[12] energy dependent fluence to effective dose conversion coefficient for particle of type k, $E_{k,i}$ is the energy of the particle i, type k recorded at the sensitive volume, and f_{E_p} is the energy use factor for the proton beam energy being considered. The total effective dose is the sum over all proton beam energies. No gantry use factors were required as the beamline being considered is a fixed beam.

3 | RESULTS

3.1 | Secondary particle yield

The energy-dependent yield of secondary particles from a 330-MeV proton beam incident on a water target over the complete 4π geometry is shown in Figure 2. Corresponding particle yields were also calculated for 250- and 190-MeV proton beams; however, pion yields were not considered for the lower proton beam energies.

3.2 | Ambient dose rates

Instantaneous dose rates arising from the fluence of various secondary particle types generated by a 330-MeV proton beam at 1.6 pA (1×10^7 p/s) beam current are shown in Figure 3. Proton beam loss points in the accelerator, beamline bending magnets, and absorption at isocenter are included. Total dose rates are primarily due to neutron fluence. No muon or pion fluence was

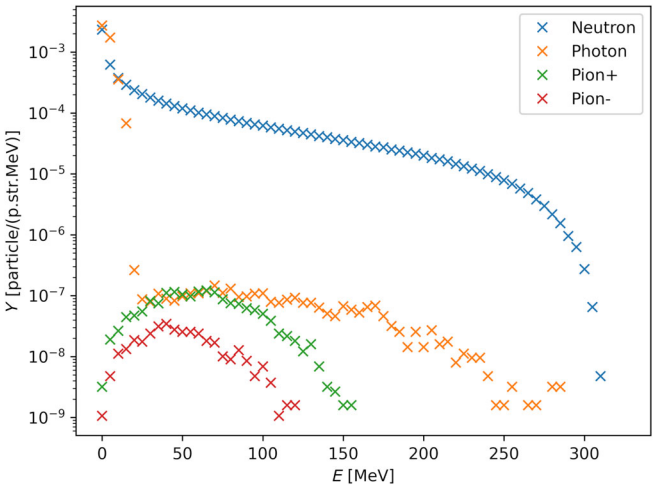

FIGURE 2 Energy spectrum of secondary particle yield for 330-MeV protons incident on a water target

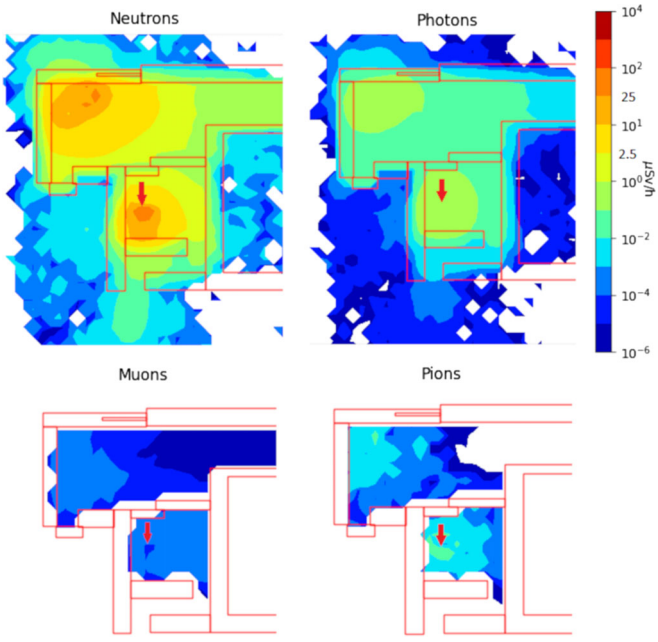

FIGURE 3 Instantaneous dose rates arising from different secondary particle fluences produced by 330-MeV protons. Outline of shielding walls are shown in red. Direction of proton beam at isocenter shown with red arrow

detected outside the shielded area. With a 330-MeV proton beam incident on a water-like material, neutron dose rates are approximately two orders of magnitude larger than photon dose rates at the maze entry.

Instantaneous dose rate maps for various proton beam energies are shown in Figure 4. The increasing yield and maximum energy of secondary neutrons as proton beam energy is increased is reflected in dose rates at the maze entry. Dose rates at the maze entry were 0.008, 0.02, and 0.07 μSv/h at proton beam energies of 190, 250, and 330 MeV, respectively. The regulatory limits for instantaneous dose rate at the facility are 50 μSv/h at the maze entry and reduce to 5 μSv/h in locations that can be occupied by members of the public for anything other than a short period of time. Therefore, instantaneous dose rates at the beam currents used for proton imaging at all locations outside the shielded area are well below regulatory limits. If proton imaging detector efficiency can be improved, proton beam currents of up to 0.1 nA could be utilized while still adhering to radiation shielding regulatory limits.

3.3 | Annual effective dose

Annual effective dose around the fixed beam room as calculated with Equation (2) is shown in Figure 5. Effective dose due to proton imaging alone and effective dose due to therapy and imaging is illustrated. The addition of high-energy proton imaging contributes negligibly to the effective dose resulting from therapy. In this scenario, effective dose due to proton imaging was approximately two orders of magnitude less than the effective dose due to proton therapy. Despite the beamline opposing the entry to the treatment room maze, the calculated annual effective doses of 0.8 mSv at the maze entry is well below the regulatory limit of 20 mSv for radiation workers.

4 | DISCUSSION

Proton imaging requires the use of higher energy proton beams than those utilized for treatment at a given anatomical location. The dependence of secondary particle yield and energy spectrum on proton beam energy means that a dedicated assessment of radiation shielding for proton imaging applications is warranted. When considering instantaneous dose rates, it has been demonstrated in this work that the increased yield at the higher proton beam energies required for imaging is offset by the lower proton beam currents required to match proton imaging detector capabilities. Therefore, the radiation shielding designed for proton therapy is more than adequate for proton imaging in terms of instantaneous dose rates.

Similarly, when considering annual doses, the increased yield of secondary particles with the use of higher proton beam energies is offset by the small number of protons required to generate a pCT image, relative to the number required in a typical treatment fraction of 2 Gy. Even in our conservative assumption of acquiring a pCT image every fraction, the proton imaging workload was calculated to be less than 0.2% of the treatment workload.

Although NCRP 144 recommends the consideration of pion production for proton beam energies greater

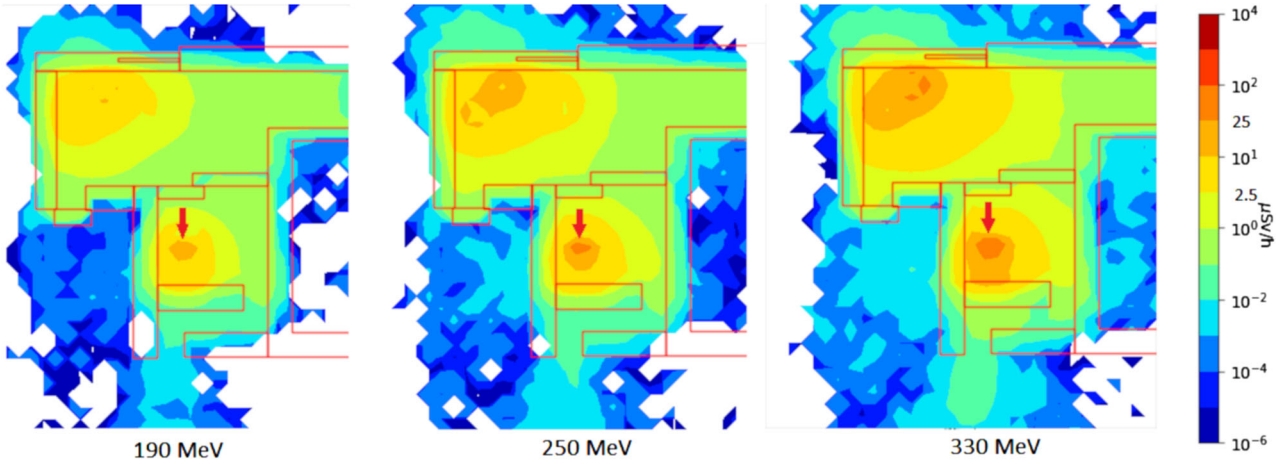

FIGURE 4 Instantaneous dose rate at 190-, 250-, and 330-MeV proton beam energies. Proton beam loss points in the accelerator, beamline bending magnets, and absorption at isocenter are included. Direction of proton beam at isocenter shown with red arrow

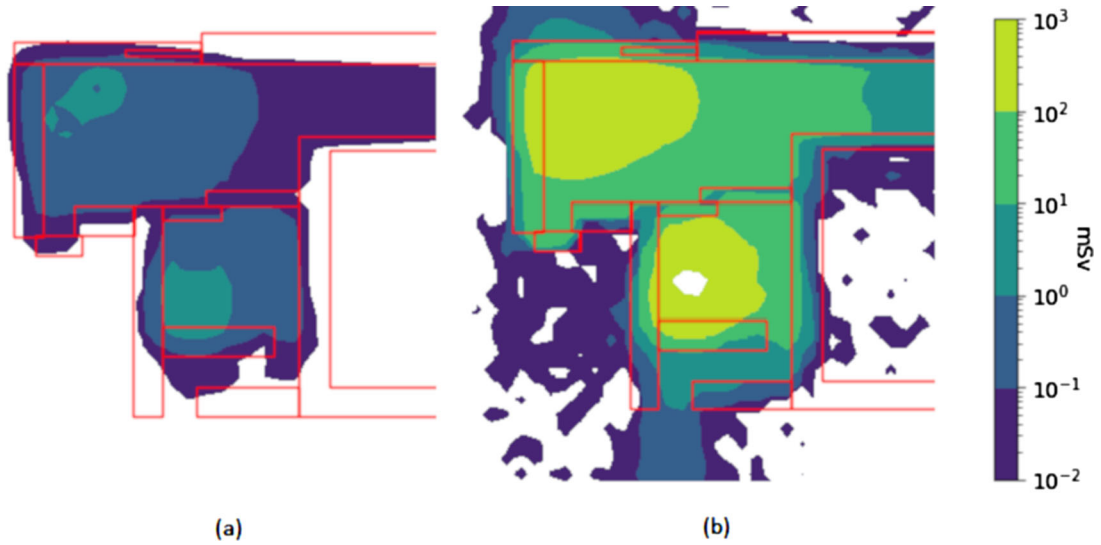

FIGURE 5 Annual effective dose estimate as a result of (a) proton imaging workload and (b) proton therapy and imaging workload

than 300 MeV, the results presented here demonstrate that pion and muon contribution to dose rates outside shielded areas is negligible at 330 MeV.

The radiation shielding assessment performed in the current work was related to a fixed beamline with upright patient positioning. Integration with gantry systems is likely required for proton imaging to become a mainstream tool for adaptive proton therapy. The relatively large, bulky detectors and the desire to remove at least the pre-patient proton tracker from the beam path during treatment mean there are still several logistical challenges to be overcome before proton imaging with modern detector systems is feasible on gantry systems. However, it can be reasonably assumed that the shielding for proton therapy treatment with a gantry system will be adequate for high-energy proton imaging based on the results presented in this work.

5 | CONCLUSION

An assessment of radiation shielding for an upright patient positioning system on a fixed beamline with proton imaging capabilities was performed in Geant4. In general, the addition of proton imaging had a negligible impact on instantaneous dose rate or annual effective dose estimates. Dose contributions due to the creation of pions by the high-energy proton imaging beam at 330 MeV were negligible in comparison to dose rates due to neutrons and photons. The shielding design for

proton therapy was adequate for the addition of proton imaging.

ACKNOWLEDGMENTS

The author acknowledges Dr Alexandre Santos for his comments on the manuscript and Dr Michael Douglass for his graphical rendering of the shielding design.

Open access publishing facilitated by The University of Adelaide, as part of the Wiley - The University of Adelaide agreement via the Council of Australian University Librarians.

CONFLICT OF INTEREST

The author declares that there is no conflict of interest that could be perceived as prejudicing the impartiality of the research reported.

REFERENCES

1. Cormack AM. Representation of a function by its line integrals, with some radiological applications. *J Appl Phys*. 1963;34(9):2722-2727. doi:10.1063/1.1729798
2. Poludniowski G, Allinson NM, Evans PM. Proton radiography and tomography with application to proton therapy. *Br J Radiol*. 2015;88(1053):20150134. doi:10.1259/bjr.20150134
3. NCRP 144. *Radiation Protection for Particle Accelerator Facilities*. National Council on Radiation Protection and Measurements; 2007.
4. DeJongh DF, DeJongh EA, Rykalin V, et al. A comparison of proton stopping power measured with proton CT and x-ray CT in fresh post-mortem porcine structures. *Med Phys*. 2021;48:7998-8009. doi:10.1002/mp.15334
5. Berger M, Coursey J, Zucker M. ESTAR, PSTAR, and ASTAR: Computer programs for calculating stopping-power and range tables for electrons, protons, and helium ions (version 1.21). 1999; http://physics.nist.gov/Star. (Accessed November 25, 2021)
6. Agostinelli S, Allison J, Amako K, et al. Geant4—a simulation toolkit. *Nucl Instrum Methods Phys Res A: Accel Spectrom Detec Assoc Equip*. 2003;506(3):250-303. doi:10.1016/S0168-9002(03)01368-8
7. Jarlskog CZ, Paganetti H. Physics settings for using the Geant4 toolkit in proton therapy. *IEEE Trans Nucl Sci*. 2008;55(3):1018-1025. doi:10.1109/TNS.2008.922816
8. Ivanchenko VN. Geant4: physics potential for instrumentation in space and medicine. *Nucl Instrum Methods Phys Res A: Accel Spectrom Detec Assoc Equip*. 2004;525(1):402-405. doi:10.1016/j.nima.2004.03.104
9. Bungau A, Cywinski R, Bungau C, King P, Lord J. Geant4 validation studies at the ISIS muon facility. Proceedings of IPAC '10, Kyoto, Japan; 2010:247-249.
10. Koi T. Shielding benchmarks for Geant4 version 10. Proceedings, 12th Meeting of Task-Force on Shielding Aspects of Accelerators, Targets and Irradiation Facilities (SATIF-12); 2015:269-275.
11. International Commission on Radiation Units and Measurements. ICRU report 95: Operational quantities for external radiation exposure. *Journal of the ICRU*. 2020.
12. International Commission on Radiological Protection. ICRP publication 116: Conversion coefficients for radiological protection quantities for external radiation exposures. *Annals of the ICRP*. 2010; 40(2-5).

How to cite this article: Penfold SN. Radiation shielding assessment of high-energy proton imaging at a proton therapy facility. *Med Phys*. 2022;49:5340–5346. https://doi.org/10.1002/mp.15727